Structural and electronic properties of expanding fluid metals

2008 J. Phys.: Condens. Matter 20 114102

(http://iopscience.iop.org/0953-8984/20/11/114102)

IOP PUBLISHING JOURNAL OF PHYSICS: CONDENSED MATTER

J. Phys.: Condens. Matter **20** (2008) 114102 (6pp) doi:10.1088/0953-8984/20/11/114102

Structural and electronic properties of expanding fluid metals

K Tamura[1], **K Matsuda**[1] **and M Inui**[2]

[1] Graduate School of Engineering, Kyoto University, Kyoto 606-8501, Japan
[2] Graduate School of Integrated Arts and Sciences, Hiroshima University, Higashi-Hiroshima 739-8521, Japan

E-mail: tamura@materials.mbox.media.kyoto-u.ac.jp

Received 30 August 2007
Published 20 February 2008
Online at stacks.iop.org/JPhysCM/20/114102

Abstract

It has been theoretically predicted that interacting electron gas suffers a negative compressibility when the electron density is sufficiently reduced. Dielectric anomaly is another expression of compressional instability in which the static dielectric function of electron gas changes sign from positive to negative. In a medium with a negative dielectric function, like charges can attract. Expanding fluid alkali metals are the ideal system in which such instability of electron gas can be probed via the structural response of ions. We have performed x-ray diffraction and small angle x-ray scattering measurements using synchrotron radiation for expanding fluid rubidium and cesium. On the basis of the experimental results we discuss the existence of compressional instability and dielectric anomaly in three-dimensional electron gas.

1. Introduction

The expansion of a metal makes it possible to reduce the density of conduction electrons. Fluid metals serve as unique materials which can be substantially expanded by heating and applying pressure to suppress boiling. With decreasing density of ions and eventually decreasing density of electrons, the free-electron-like behavior of electrons is dramatically changed.

Expanding fluid metals such as mercury (Hg), rubidium (Rb) and cesium (Cs) have been extensively investigated in the last two decades [1]. The liquid–gas critical points of these metals (Hg: $T_c = 1751$ K, $P_c = 167.3$ MPa [2]; Rb: 2017 K, 12.45 MPa [3]; Cs: 1924 K, 9.25 MPa [3]) are rather low and accessible using the laboratory techniques of high temperature and high pressure which enable the density of fluid metals to decrease substantially and continuously from the liquid to the rarefied vapor. In the studies of expanding fluid metals attention has been mostly paid on the metal–nonmetal (M–NM) transition which takes place near the critical point. In fluid Hg it is known that the M–NM transition occurs approximately at the density of 9 g cm^{-3} which is rather large compared with the critical density of 5.85 g cm^{-3} [2]. In fluid Rb and Cs the M–NM transition occurs around 0.29 and 0.38 g cm^{-3}, respectively, which values coincide with their critical densities [3].

Experimental studies on electronic and thermodynamic properties of fluid Hg have been widely made and the aspect of the M–NM transition has been clarified. Recently, static and dynamic structures of fluid Hg over a wide density range have been investigated by the present authors using synchrotron radiation [4–6]. It was revealed that the M–NM transition is accompanied by a structural instability in which a nanoscale fluctuation with a relaxation time of several picoseconds occurs. The structural investigation suggested that the behavior of low density electrons in the vicinity of the M–NM transition strongly affects those of ions and plays a crucial role in determining the thermodynamic nature of the transition. Regarding fluid Rb and Cs, electronic and thermodynamic properties as well as structural ones [7–9] have been investigated. It has been widely recognized that there appear anomalous behaviors in electronic properties such as an enhancement of magnetic susceptibility prior to the M–NM transition [7]. Also an interesting result was obtained by the measurement of inelastic neutron scattering for fluid Rb [10], suggesting that diatomic molecules (dimers such as Rb_2) exist in the metallic state near the critical point.

Apart from the M–NM transition, we have another important subject, concerning the instability of low density electron gas, which could be examined by the use of expanding fluid metals. Since Wigner's pioneering work [11], anomalous behaviors of low density electron gas have been extensively investigated, particularly in the search for new materials such as superconductors with a non-phonon process [12, 13]. The

unique properties of low density electron gas have been discussed on the basis of ground-state energy, which is conventionally given as a function of the expansion parameter r_s (r_s is the Wigner–Seitz radius in units of Bohr radius). One of the most remarkable properties is the compressional instability; the compressibility of the electron gas changes its sign from positive to negative [14, 15] with decreasing electron density, which was theoretically predicted to occur when $r_s > 5.25$. This means that the electron gas is unstable against collapse at lower densities. Negative compressibility is closely related to the negative sign of the electron static dielectric function (DF), $\varepsilon(\mathbf{q}, 0)$, at a small $|\mathbf{q}|$ by taking the compressibility sum rule into account [16]. The negative sign of the static DF of electron gas leads to an unusual situation in which test charges with the same sign, either positive or negative, attract in a medium of electron gas with a static negative DF. The negative sign of the static DF of electron gas is theoretically possible without violating any causality or stability requirements, and appears only if the exchange and correlation effects are taken into account [17]. Here, a question arises as to whether the negative sign of the static electron DF really exists and is observable in real systems such as metals. Although the existence of the negative electron DF has been reported thus far in a synthesized two-dimensional system such as the interface between semiconductors [18], the existence of the negative electron DF in a three-dimensional system has never been confirmed.

Fluid alkali metals are ideal materials for solving the problem of electron gas instability for the following reasons. First, alkali metals are typical prototypes of three-dimensional electron gas because of their almost spherical Fermi surface. Second, a continuous and substantial reduction in electron density is possible, by utilizing volume expansion along the liquid–vapor saturation line. Third, positive ions in fluids can readjust their position easily compared with those in solids; thus structural change might be more pronouncedly observed in fluids through the coupling of electrons and ions when the instability of electron gas occurs.

In the present paper, we review recent results of x-ray diffraction (XD) and small angle x-ray scattering (SAXS) measurements for fluid Rb [19] and report new results for Cs. On the basis of these results we discuss the instability of electron gas.

2. Experimental details

To solve the problem of electron instability it is necessary to overcome experimental difficulties arising from very high critical temperatures and pressures and to perform precise structural measurements. In particular, the absence of a sample container has made it difficult to perform such experiments on expanded fluid alkali metals. We have recently devised a sample cell with x-ray windows made of single-crystalline molybdenum resistant to the high reactivity of hot alkali metals [20]. By combining this cell with a high pressure apparatus [21], we have succeeded in measuring the XD and SAXS of fluid alkali metals over a wide range of temperatures and pressures from the triple point up to supercritical regions.

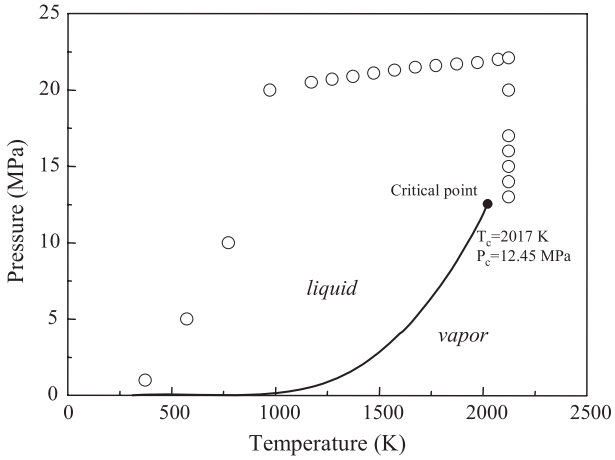

Figure 1. Phase diagram of rubidium ($T_c = 2017$ K, $P_c = 12.45$ MPa) in which open circles indicate the temperatures and pressures at which experiments were performed.

We have obtained precise structural data using a synchrotron radiation source.

The XD measurements were carried out in the energy-dispersive mode at the BL28B2 beamline at SPring-8 in Japan. White x-rays were used as the incident beam, and scattered x-rays were detected using a pure-germanium solid-state detector. SAXS measurements were performed at the BL04B2 beamline at SPring-8. Monochromatized 38 keV x-rays were used as the incident beam and scattered x-rays were detected using an imaging plate. Stable and precise measurements were carried out up to 2123 K and 22.0 MPa beyond the critical point for Rb and up to 1923 K and 15.0 MPa for Cs. The SAXS measurements were made on the beamline BL04B2 at SPring-8. 38 keV x-rays monochromatized using flat Si(111) were collimated to 0.2×0.2 mm^2 via the horizontal and vertical slits located in the optical hutch and then incident on the sample. The scattered x-rays were detected using an imaging plate with a camera length of about 2960 mm. A vacuum path was mounted between the sample stage and the imaging plate to reduce background from the air.

3. Results

3.1. Rubidium

Figure 1 shows the phase diagram of Rb in which open circles indicate the temperatures and pressures at which the present XD and SAXS measurements were performed. The structure factor $S(Q)$ for fluid Rb is plotted at different temperatures, pressures and densities in figure 2. The $S(Q)$ data in the low Q region were obtained by SAXS measurement separately carried out. With increasing temperature and decreasing density, the intensities of both the first and second maxima decrease. However, the overall oscillatory structure persists even in the high temperature region of up to 2123 K. As seen in the figure, the first maximum slightly shifts to a lower Q with decreasing density. In contrast, the second peak of $S(Q)$, which is not completely blurred out, shifts to a region of relatively high Q. In addition, the $S(Q)$ at a low Q less than

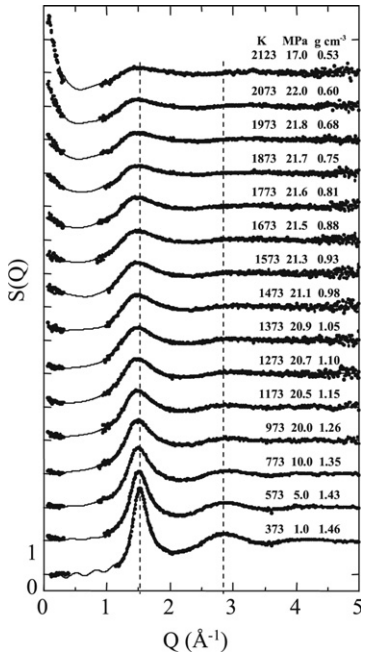

Figure 2. Structure factors $S(Q)$ for expanded fluid rubidium at various temperatures and pressures. Temperature, pressure and density are indicated on the upper right-hand side of each data set. The dots represent the experimental data and the full curves show the Fourier transforms of $g(R)$ in figure 3. The position of the second maximum shifts to relatively high Q values from 2.8 Å^{-1} at 1.46 g cm^{-3} to 3.3 Å^{-1} at 0.53 g cm^{-3}, whereas that of the first maximum shifts to relatively low Q values from 1.52 Å^{-1} at 1.46 g cm^{-3} to 1.46 Å^{-1} at 1.05 g cm^{-3} and remains at approximately 1.46 Å^{-1} with further density reduction.

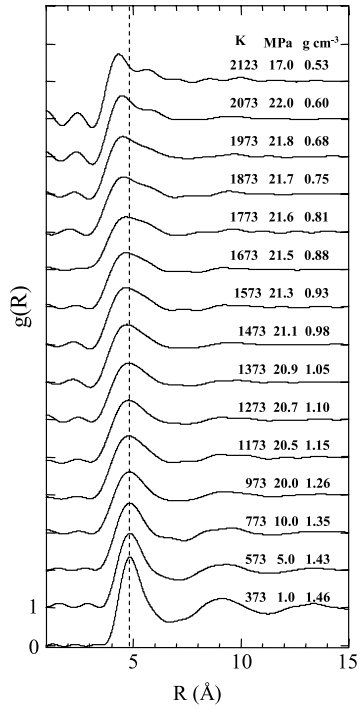

Figure 3. Pair distribution function $g(R)$ of fluid rubidium derived from Fourier transform of $S(Q)$. The broken line denotes the peak position of the first maximum of $g(R)$ at 373 K. Temperature, pressure and density are indicated on the upper right-hand side of each curve.

0.3 Å^{-1} starts to increase with decreasing Q at a density of approximately 1.0 g cm^{-3}. The pair distribution function $g(R)$ is deduced from the Fourier transform of $S(Q)$ and is shown in figure 3. The peak height of the first maximum of $g(R)$ progressively decreases, whereas that of the second maximum approaches 1. Note that the position of the first maximum starts to shift to a low R below a density of 1.1 g cm^{-3}.

The density variation of the position of the first maximum, R_1, is shown in figure 4(a). R_1 corresponds to the nearest-neighbor distance. It is located at approximately 4.85 Å at 373 K and is almost the same as that of the solid state. It remains constant with a decreasing density from 1.5 to 1.1 g cm^{-3} and then starts to decrease. It gradually decreases with further density decrease and shows saturation at approximately 4.2 Å at densities lower than 0.5 g cm^{-3}. The value of 4.2 Å is nearly equal to the bond length of a dimer in the vapor [22].

Figure 4(b) shows the density variation in coordination number N_1 which is derived by integrating the radial distribution function defined by $4\pi R^2 n_0 g(R)$ (n_0: number density) up to the first-minimum position. N_1 decreases substantially and almost linearly with decreasing density from 1.5 to 1.1 g cm^{-3} and then shows a strong deviation from a linear dependence, remaining at approximately 6 until 0.7 g cm^{-3} is reached.

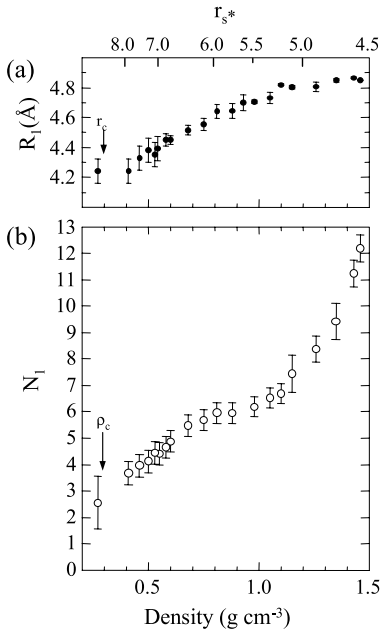

Figure 4. Density variation of the local structure of fluid rubidium: (a) the average interatomic distance R_1, (b) the coordination number N_1. The critical density is denoted ρ_c. The corresponding scale of r_s^* is shown on the upper axis of the graph of R_1.

As shown in figure 2 the $S(Q)$ at a low Q less than 0.3 Å^{-1} starts to increase with decreasing Q, which indicates the appearance of density fluctuation. We derived the correlation length ξ and $S(0)$ using the Ornstein–Zernike

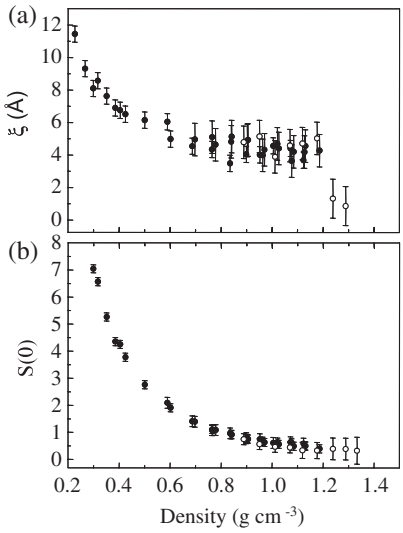

Figure 5. Density variation of the correlation length ξ and $S(0)$ for expanded fluid rubidium up to the critical region. Dots represent the data measured at the conditions shown in figure 1. Open circles indicate the data measured at the pressure of 5 MPa.

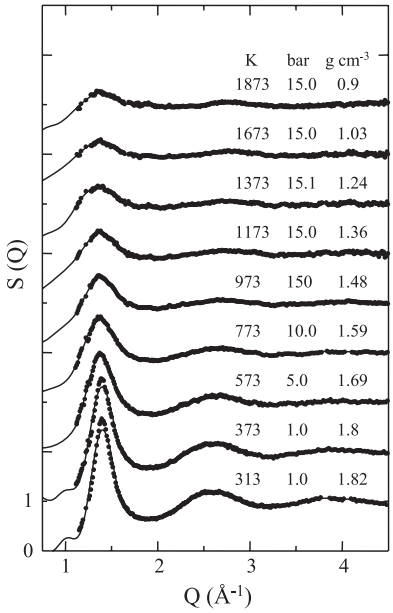

Figure 6. Structure factors $S(Q)$ for fluid cesium at various temperatures and pressures. Temperature, pressure and density are indicated on the upper right-hand side of each data set. The dots represent the experimental data and the full curves show the Fourier transforms of $g(R)$ in figure 7.

formula. Figure 5(a) shows the density variation of ξ which is about 5 Å approximately at 1.2 g cm^{-3} and remains almost constant in the density range from 1.2 to 0.6 g cm^{-3}. The density range coincides with the range in which anomalous behaviors were observed in the data as shown in figure 4. Then it substantially increases below 0.6 g cm^{-3} as the density of the fluid approaches the critical density. Figure 5(b) shows the density variation of $S(0)$ which gradually increases with decreasing density and is observable in the density range from 1.2 to 0.6 g cm^{-3}. Then it shows a substantial increase below 0.6 g cm^{-3} as the density of the fluid approaches the critical density. In figure 5 we present the data at different pressures: dots represent the data measured at the condition shown in figure 1 and open circles indicate the data measured at pressure of 5 MPa which is much lower than the critical pressure. It should be noticed that the data at 5 MPa are completely the same as the data indicated by closed circles, which indicates that the appearance of density fluctuation around 1.1 g cm^{-3} is not interpreted as a tail of the critical one.

3.2. Cesium

Figure 6 shows $S(Q)$ for fluid Cs at different temperatures, pressures and densities. With increasing temperature and decreasing density, the intensities of both the first and second maxima decrease. As seen in the figure, the first maximum slightly shifts to a lower Q with decreasing density. In contrast, the second peak of $S(Q)$, which is not completely blurred out, shifts to a relatively higher Q region. Figure 7 shows $g(R)$. The peak height of the first maximum of $g(R)$ progressively decreases, whereas that of the second maximum approaches 1. Note that the position of the first maximum starts to shift to a low R below a density of 1.3 g cm^{-3}. The density variations of R_1 and N_1 are shown in figures 8(a) and (b), respectively. As seen in figure 8(a), R_1 slightly decreases and remains

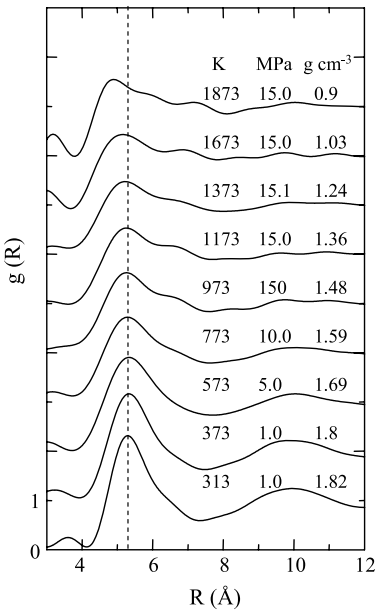

Figure 7. Pair distribution function $g(R)$ of fluid cesium derived from Fourier transform of $S(Q)$. The broken line denotes the peak position of the first maximum of $g(R)$ at 350 K. Temperature, pressure and density are indicated on the upper right-hand side of each curve.

almost constant with decreasing density from 1.8 to 1.3 g cm^{-3} and then starts to decrease around 1.3 g cm^{-3}. N_1 decreases substantially and almost linearly with decreasing density from 1.8 to 1.3 g cm^{-3} and then shows a slight deviation from a linear dependence. These overall features for fluid Cs are quite

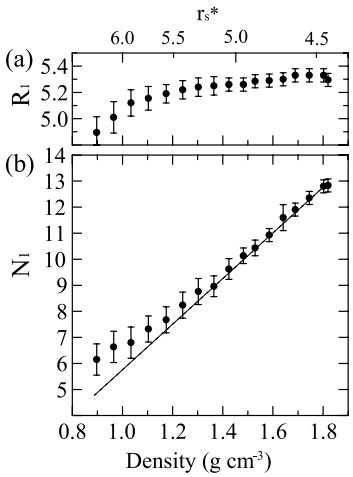

Figure 8. Density variation of the local structure of fluid cesium: (a) the mean interatomic distance R_1, (b) the coordination number N_1. The corresponding scale of r_s^* is shown on the upper axis of the graph of R_1.

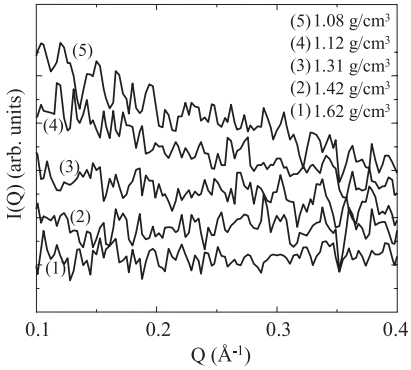

Figure 9. SAXS spectra for fluid Cs with decreasing density. The intensity starts to increase around 1.3 g cm^{-3}.

similar to those for Rb, except the difference in densities at which the structural changes start to occur. As seen in figure 9, the SAXS results also show that a weak scattering starts to appear approximately at 1.3 g cm^{-3}.

4. Discussion

The structural change observed in the density range from 1.1 to 0.5 g cm^{-3} for Rb as shown in figure 4(a) is quite opposite to that expected because interatomic distance decreases despite mean interatomic distance increasing with volume expansion. Such a structural change is also opposite to the previous results obtained from neutron diffraction measurements for Rb [8] as well as Cs [9] in which R_1 rather increases with decreasing density. In these pioneering works of neutron diffraction, $S(Q)$ was not obtained in the high Q region, there especially being a lack of data on the second maxima in $S(Q)$ which is important for obtaining the precise R_1. The structural features in the present results strongly indicate that an attractive force appears to work among ions in the density range from 1.1 to 0.5 g cm^{-3}. As seen in figure 4(b) the coordination number shows a deviation from a linear decrease and is maintained constant in the range from 1.1 to 0.7 g cm^{-3} in spite of progressive expansion, which indicates the appearance of a spatial inhomogeneity. As seen in figures 5(a) and (b) the density fluctuation, which is weak but independent of the critical scattering, was clearly observed in the corresponding density range. Such inhomogeneity was also found in the *ab initio* molecular dynamics simulation of liquid rubidium by Shimojo *et al* [23] and the Monte Carlo simulation by Chacon *et al* [24].

It is critical that local structural parameters, R_1 and N_1, be scaled by the expansion parameter r_s. In real systems such as metals, the effect of core polarization by ions reduces the strength of the effective interaction among electrons. Kukkonen *et al* pointed out that an ionic background can be viewed as a uniform and polarizable background by taking core polarizability to be a constant. Thus, r_s for the electron gas in metals should be scaled with $r_s^* = r_s/\epsilon_B$ rather than with r_s, where ϵ_B is the dielectric constant of the polarizable background defined by $\epsilon_B = 1 + 4n\alpha$ (α: ionic polarizability, n: the number density of ions) [25]. This corrected r_s ($= r_s^*$) is shown on the upper horizontal axis of figure 4(a). As seen in the figure, R_1 starts to decrease and N_1 shows a deviation from a linear decrease between $r_s^* = 5$ and 5.5. This density range agrees well with the critical r_s (=5.25) beyond which the compressibility of electron gas becomes negative and also the static electron DF becomes negative at a low wavevector. The negative electron DF generates an attractive Coulomb interaction among test charges with the same sign, either electrons themselves or ions. However, this does not immediately lead to a spontaneous self-compression of the whole system [26] because the stability is sustained by the compensating positive charges. The observed local contraction in the metallic state below 1.1 g cm^{-3} can be interpreted as structural variation caused by the enhancement in the attractive force among the ions.

The local contraction indicates an increase in local atomic density, which would generate a rare region of density at the same time. It would be natural to consider that the density fluctuation observed in the present SAXS measurements is induced by the instability of a low density electron gas. In fact, it has been suggested by Pines and Nozieres [27] for the jellium model that the negative sign of the electron DF might lead to instability of the ion system; if the constraint of a uniform rigid background is eliminated, the condition $\varepsilon(\mathbf{q}, 0) < 0$ brings about a spontaneous density fluctuation of the background with corresponding $|\mathbf{q}|$. In the fluids, the ions can rearrange their position easily compared with those in solids. The density fluctuation in the range from 1.1 to 0.6 g cm^{-3} might be related to the instability of the electron gas; the density fluctuation takes place when the instability of electron gas starts to be eliminated by structural response of ions, which strongly indicate the existence of the negative static DF of electron gas in expanded fluid alkali metals.

XD results for fluid Cs are quite suggestive. The density of 1.3 g cm^{-3} around which R_1 starts to decrease with decreasing density is almost the same density as corresponds to the critical r_s (=5.25) when the polarization effect of Cs ions is taken

into account. The density fluctuation also appears around the same region. These facts indicate that the structural changes in fluid Cs also originate from the instability of electron gas. The common features observed in Rb and Cs have the same origin, which confirms the existence of the compressional instability of the low density electron gas and gives the evidence for the existence of negative static DF which has been theoretically predicted but never proved experimentally.

On the basis of the idea mentioned above, it is interesting to see the other experimental data on expanding fluid Rb and Cs. It has been recognized that anomalous behaviors in electronic and thermodynamic properties start to appear in the metallic region which is not so far from the melting point; the deviation from the nearly free-electron behavior [1], the enhancement of magnetic susceptibility [7] and the increase of inner pressure [28]. The density from which such anomalous behaviors start to occur is exactly the same as that corresponding to the critical r_s (=5.25).

As mentioned in section 1 the results of inelastic neutron scattering measurements for fluid Rb suggested that dimers (Rb_2) exist in the metallic state prior to the M–NM transition [10]. Since Rb_2 is known to exist in the rarefied vapor as a main constituent, it is not unreasonable to consider the coexistence of two types of electrons with covalent and metallic nature in the metallic state. However, the structural change observed in the present experiments does not mean the appearance of dimers, but more appropriately speaking, the fluctuation of local structure originated from the instability of low density electron gas. It might be constructive to reconsider the origin of dimers in connection with the instability of the electron gas. Also, it might be meaningful to consider the M–NM transition along the same line.

5. Conclusion

We have performed x-ray diffraction and small angle x-ray scattering measurements using synchrotron radiation for expanding fluid Rb and Cs and obtained experimental evidence for the existence of compressional instability and negative static dielectric function (DF) in the low density electron gas. Theoretical efforts have been made to understand the physical meaning of the negative DF of electron gas from the microscopic point of view [29, 30]. The negative sign of the static electron DF is of great importance for causing an attractive Coulomb interaction among electrons, when electrons are regarded as test charges, which raises the possibility of electron pairing. Thus, the negative static DF in the electron system is quite important when considered for producing a new type of superconductor. Various theories have predicted that the negative static DF is closely associated with the appearance of high T_c superconductivity [31].

Acknowledgments

The authors are grateful to Professor Y Takada for helpful discussion and comments. The authors also thank Drs K Kato and S Kohara of SPring-8, and S Mukaimoto, K Naruse and K Hayasi for technical support. The synchrotron radiation experiments were performed at the SPring-8 with the approval of the Japan Synchrotron Radiation Research Institute (JASRI). This work was supported by a Grant-in-Aid for Scientific Research Fund from the Ministry of Education, Culture, Sports, Science and Technology (Research Nos 11102004 and 16760532). The authors thank Mr M Katoh of Allied Material Corporation for his cooperation in fabricating the cell and supplying the molybdenum crystals made in the company.

References

[1] Hensel F and Warren W W Jr 1999 *Fluid Metals. The Liquid–Vapor Transition of Metals* (Princeton, NJ: Princeton University Press)
[2] Gaetzlaf W 1988 *PhD Thesis* University of Marburg
[3] Juengst S, Knuth B and Hensel F 1985 *Phys. Rev. Lett.* **55** 2160
[4] Inui M, Hong X and Tamura K 2003 *Phys. Rev.* B **68** 094108
[5] Ishikawa D, Inui M, Matsuda K, Tamura K, Tsutsui S and Baron A Q R 2004 *Phys. Rev. Lett.* **93** 097801
[6] Inui M, Matsuda K, Ishikawa D, Tamura K and Ohishi Y 2007 *Phys. Rev. Lett.* **98** 185504
[7] Freyland W 1980 *Phys. Rev.* B **20** 5104
[8] Franz G, Freyland W, Glaeser W, Hensel F and Schneider E 1980 *J. Physique Coll.* **C8** 194
[9] Winter R, Hensel F, Bodensteiner T and Glaeser W 1987 *Phys. Chem.* **91** 1327
[10] Pilgrim W C, Ross M, Yang L H and Hensel F 1997 *Phys. Rev. Lett.* **78** 3685
[11] Wigner E P 1934 *Phys. Rev.* **46** 1002
[12] Kohn W and Luttinger J M 1965 *Phys. Rev. Lett.* **15** 524
[13] Takada Y 1989 *Phys. Rev.* B **39** 11575
[14] Mahan G D 2000 *Many-Particle Physics* (New York: Kluwer–Academic/Plenum)
[15] Ceperley D M and Alder B J 1980 *Phys. Rev. Lett.* **45** 566
[16] Giuliani G and Vignale G 2005 *Quantum Theory of the Electron Liquid* (Cambridge: Cambridge University Press)
[17] Dolgov O V, Kirzhnits D A and Maksimov E G 1981 *Rev. Mod. Phys.* **53** 81
[18] Eisenstein J P, Pfeiffer L N and West K W 1992 *Phys. Rev. Lett.* **68** 674
[19] Matsuda K, Tamura K and Inui M 2007 *Phys. Rev. Lett.* **98** 096401
[20] Matsuda K, Tamura K, Katoh M and Inui M 2004 *Rev. Sci. Instrum.* **75** 709
[21] Tamura K and Inui M 2001 *J. Phys.: Condens. Matter* **13** R337
[22] Miroslav U, Andrzej J and Sadlej J 1995 *J. Chem. Phys.* **103** 9692
[23] Shimojo F, Zempo Y, Hoshino K and Watabe M 1995 *Phys. Rev.* B **52** 9320
[24] Chacon E, Reinaldo-Falagan M, Tarazona P, Velasco E and Hernandez J P 2005 *Phys. Rev.* B **71** 024204
[25] Kukkonen C A and Wilkins J W 1979 *Phys. Rev.* B **19** 6075
[26] Ichimaru S 1982 *Rev. Mod. Phys.* **54** 1017
[27] Pines D and Nozieres P 1966 *The Theory of Quantum Liquids* vol 1 (New York: Benjamin)
[28] Hensel F 1982 *Proc. 8th Symp. on Thermodynamic Properties* ed J Sengers (New York: ASME) p 151
[29] Takada Y 2005 *J. Supercond.* **18** 185
[30] Takayanagi K and Lipparini E 1997 *Phys. Rev.* B **56** 4872
[31] Tachiki M, Machida M and Egami T 2003 *Phys. Rev.* B **67** 174506